Alexandria Engineering Journal (2022) 61, 3323–3333

Alexandria University

Alexandria Engineering Journal

www.elsevier.com/locate/aej
www.sciencedirect.com

MHD mixed convection flow of a hybrid nanofluid past a permeable vertical flat plate with thermal radiation effect

Nur Syahirah Wahid [a], Norihan Md Arifin [a,b], Najiyah Safwa Khashi'ie [c], Ioan Pop [d,*], Norfifah Bachok [a,b], Mohd Ezad Hafidz Hafidzuddin [e]

[a] *Department of Mathematics, Faculty of Science, Universiti Putra Malaysia, 43400 UPM Serdang, Selangor, Malaysia*
[b] *Institute for Mathematical Research, Universiti Putra Malaysia, 43400 UPM Serdang, Selangor, Malaysia*
[c] *Fakulti Teknologi Kejuruteraan Mekanikal dan Pembuatan, Universiti Teknikal Malaysia Melaka, Hang Tuah Jaya, 76100 Durian Tunggal, Melaka, Malaysia*
[d] *Department of Mathematics, Babeş-Bolyai University, R-400084 Cluj-Napoca, Romania*
[e] *Centre of Foundation Studies for Agricultural Science, Universiti Putra Malaysia, 43400 UPM Serdang, Selangor, Malaysia*

Received 23 June 2021; revised 25 July 2021; accepted 20 August 2021
Available online 03 September 2021

KEYWORDS

Mixed convection;
Hybrid nanofluid;
Vertical flat plate;
Radiation;
Stability analysis

Abstract The magnetohydrodynamic (MHD) radiative flow of a hybrid alumina-copper/water nanofluid past a permeable vertical plate with mixed convection is the focal interest in this present work. Dissimilar to the traditional nanofluid model that considers only one type of nanoparticles, we consider the hybridization of two types of nanoparticles in this work which are alumina and copper. The governing flow and heat transfer equations are simplified to the ordinary differential equations (ODEs) with the adaptation of conventional similarity transformations which are then evaluated by the bvp4c solver (MATLAB) to generate the numerical solutions. The solutions are generated and illustrated in the form of graph to be easily observed. Although dual solutions are obtained in this study, only one solution is determined to be stable. By reducing the concentration volume of copper and increasing the magnetic and radiation parameters, the boundary layer separation can be hindered. With the occurrence of opposing flow due to the mixed convection parameter, the heat transfer can be enhanced when the concentration volume of copper is being reduced and when the magnetic and radiation parameters are being proliferated.

1. Introduction

Traditional nanofluid is engineered by dispersing a kind of nanoparticles in a base fluid [1]. This dispersion of nano-sized particles is believed to augment the heat transfer effi-

* Corresponding author.
E-mail address: popm.ioan@yahoo.co.uk (I. Pop).
Peer review under responsibility of Faculty of Engineering, Alexandria University.

https://doi.org/10.1016/j.aej.2021.08.059

ciency of the transmitting fluid due to the special properties carried by the nanoparticles. However, the dispersion of a single type of nanoparticles is noticed to only possess limited thermophysical properties. Therefore, the researchers have established a novel generation of heat transfer fluid as the extension towards nanofluid which is called as hybrid nanofluid. This generation of nanofluid is prepared with the hybridization of dissimilar types of nanoparticles that are dispersed into the base fluid. Hybrid nanofluid is certainly having an extra specialty in the context of thermophysical properties, heat transfer performance, and stability due to the presence of a dissimilar type of nanoparticles compared to the traditional nanofluid that only possesses a single type of nanoparticles [2].

The promising influence of hybrid nanofluid have attracted many manufacturers, developers, and engineers to imply this type of heat transfer fluid towards various heat transfer application such as in heat exchanger, biomedical, electronic, generator and transformer cooling, heat pipes and refrigeration [3,4]. However, more extensive research needs to be done on this kind of heat transfer fluid so that its thermophysical and hydrodynamic properties towards a specific application can be fully understood and utilized before commercializing on a wide scale. We have seen many researchers have conducted numerous investigations on hybrid nanofluid either by using the experimental or numerical approach. There are two thermophysical correlations of hybrid nanofluid that have been commonly employed by the researchers in the numerical investigations which are those that have been suggested by Devi and Devi [5,6] (Type I) and the other one is suggested by Takabi and Salehi [7] (Type II). See also the following for the recent studies [8–20] for Type I, and [21–25] for Type II.

Moreover, a physical phenomenon of the fluid flow that is under the exertion of magnetic field is known as magnetohydrodynamic (MHD) effect. The resistive force called as Lorentz force will be intensely developed due to the presence of MHD effect in the electrically conducting fluid (e.g., salt water, liquid metals, electrolytes, and plasmas) which causes the fluid flow to be decelerated, meanwhile the temperature and the concentration of the fluid will be magnified. Therefore, the transition of the flow from laminar to turbulent state can be delayed by controlling this effect. Many researchers have applied this effect in their studies, for instance, Das et al. [26] included MHD effect in their analysis of hybrid nanofluid flow in porous channel and reported that the fluid temperature is enhanced due to the presence of MHD. Wahid et al. [27] also noted the same influence of MHD towards the temperature profile in their analytical investigation. Several other studies that consider magnetic/MHD effect in their investigation can be seen in the following literature, [28–32].

Moreover, the investigation towards the mixed convection flow in various kind of fluid also becomes a significant consideration among the researchers because of its myriad implementations in technology and industry, such as in electronic devices, nuclear reactors, and pipeline transport. Mixed convection is the combination of free convection and forced convection. Generally, convection is the process of heat transfer related to the motion of fluid from the hotter material to the colder material. Additionally, free convection is a mixing motion that is due to the difference in density, meanwhile, forced convection is a mixing motion generated by an external source. Thus, mixed convection is the combination of these two processes. Interesting studies regarding the free and forced convection flow have been extensively elucidated by Ghalambaz et al. [33–35] and Ho et al. [36] towards the new generation of hybrid nanofluid which is by using the Nano-Encapsulated Phase Change Materials (NEPCMs) to enhance the heat transfer performance.

The implementation of mixed convection towards the hybrid nanofluid flow model has currently become one of the interest investigations among the researchers due to the realization of their essentiality in a real-world application. Waini et al. [37] found out that the velocity distribution is decelerating when the mixed convection parameter is reducing in their investigation of hybrid nanofluid flow in a porous medium of a vertical surface. The same pattern of velocity profile also has been obtained by Rostami et al. [38] and Khashi'ie et al. [39] due to the mixed convection effect in their particular study. Most of the investigations regarding the mixed convection flow of hybrid nanofluid have reported that the presence of multiple solutions is due to the opposing flow of mixed convection, and the occurrence of the boundary layer separation happens at the opposing flow region [40–47].

With the contemplation on the previous literature and the limitation of findings in this research area, we are inspired to conduct the numerical investigation on the MHD radiative flow of a hybrid nanofluid past a permeable vertical plate with mixed convection. The correlation of hybrid nanofluid suggested by Takabi and Salehi [7] is implemented. We aim to discover the numerical solutions and identify the practical solution for the present problem, which hopefully provide a significant contribution towards the development of hybrid nanofluid and benefit other researchers with our final findings.

2. Mathematical model

The steady MHD mixed convection boundary layer flow of a water-based hybrid nanofluid over a vertical flat plate is considered. The physical representation of the model can be seen in Fig. 1, with the following descriptions:

- x-axis is parallel to the surface of the plate and y-axis is normal to it with the flow is at $y \geqslant 0$.
- u and v are the velocity components of the fluid along x and y axes, respectively.
- We take $T_w(x) = T_\infty + T_0(x/L)$ such that $T_w(x)$ is the surface temperature while T_∞ is the ambient temperature.
- T_0 is a characteristic temperature with $T_0 > 0$ is for assisting flow and $T_0 < 0$ is for opposing flow, respectively, and $h_f(x) = \bar{h}_f(x/L)^{-1/2}$ is the heat transfer coefficient.
- The mass flux velocity is $v_w(x)$ with $v_w(x) < 0$ for suction and $v_w(x) > 0$ for injection.
- A variable magnetic field is $B(x) = B_0(x/L)^{-1}$ where B_0 is the magnetic strength employed to the plate along the y direction and L is the plate length.
- The radiation term q_r is applied.

According to the descriptions above, the governing boundary layer equations of the present hybrid nanofluid model can be formulated as (Krishna et al. [48]; Devi and Devi [6]):

$$\frac{\partial u}{\partial x} + \frac{\partial v}{\partial y} = 0 \tag{1}$$

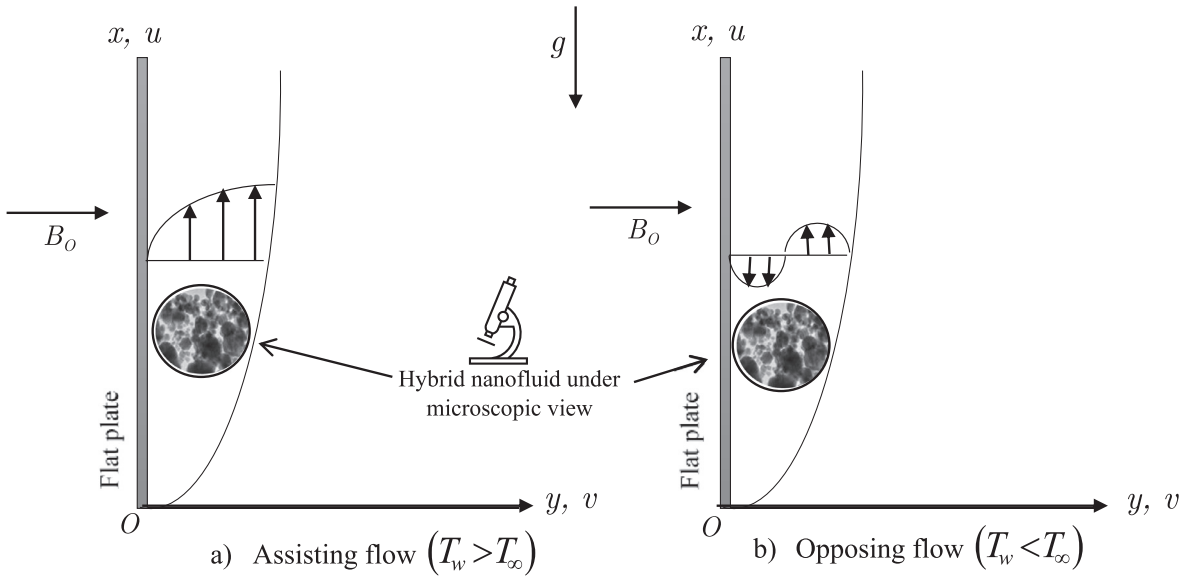

Fig. 1 Model illustration.

$$u\frac{\partial u}{\partial x}+v\frac{\partial u}{\partial y}=\frac{\mu_{hnf}}{\rho_{hnf}}\frac{\partial^2 u}{\partial y^2}-\frac{\sigma_{hnf}B_0^2}{\rho_{hnf}}u+\beta_{hnf}(T-T_\infty)g \tag{2}$$

$$u\frac{\partial T}{\partial x}+v\frac{\partial T}{\partial y}=\frac{k_{hnf}}{(\rho C_p)_{hnf}}\frac{\partial^2 T}{\partial y^2}-\frac{1}{(\rho C_p)_{hnf}}\frac{\partial q_r}{\partial y} \tag{3}$$

conditioned to

$$v=v_w(x),\ u=0,\ -k_{hnf}\frac{\partial T}{\partial y}=h_f(T_w-T)\text{at } y=0 \tag{4}$$

$$u\to 0,\ T\to T_\infty \text{ as } y\to\infty$$

As the radiation effect is implemented in the present model, the radiative heat flux q_r is equated as according to Rosseland [49] approximation (see also [50,51]):

$$q_r=-\frac{4\sigma^*}{3k^*}\frac{\partial T^4}{\partial y} \tag{5}$$

such that k^* and σ^* denote the mean absorption coefficient and the Stefan-Boltzmann constant, respectively. Adapting the Taylor series and disregarding the higher-order terms, T^4 is expanded about T_∞ to obtain $T^4\approx 4T_\infty^3T-3T_\infty^4$. Now, the energy equation can be formulated as

$$u\frac{\partial T}{\partial x}+v\frac{\partial T}{\partial y}=\frac{1}{(\rho C_p)_{hnf}}\left(k_{hnf}+\frac{16\sigma^*T_\infty^3}{3k^*}\right)\frac{\partial^2 T}{\partial y^2} \tag{6}$$

Further, μ_{hnf} is the dynamic viscosity, ρ_{hnf} is the density, k_{hnf} is the thermal conductivity, $(\rho C_p)_{hnf}$ is the heat capacity of the hybrid nanofluid and σ_{hnf} is the electrical conductivity, and β_{hnf} is the thermal expansion of hybrid nanofluid that can be specified as [7]:

$$\mu_{hnf}=\mu_f(1-\phi_{Al_2O_3}-\phi_{Cu})^{-2.5},\text{where } \phi_{hnf}=\phi_{Al_2O_3}+\phi_{Cu}, \tag{7}$$

$$\rho_{hnf}=\phi_{Al_2O_3}\rho_{Al_2O_3}+\phi_{Cu}\rho_{Cu}+(1-\phi_{hnf})\rho_f,$$

$$(\rho C_p)_{hnf}=\phi_{Al_2O_3}(\rho C_p)_{Al_2O_3}+\phi_{Cu}(\rho C_p)_{Cu}+(1-\phi_{hnf})(\rho C_p)_f,$$

$$\frac{k_{hnf}}{k_f}=\left[\left(\frac{\phi_{Al_2O_3}k_{Al_2O_3}+\phi_{Cu}k_{Cu}}{\phi_{hnf}}\right)+2k_f+2(\phi_{Al_2O_3}k_{Al_2O_3}+\phi_{Cu}k_{Cu})-2\phi_{hnf}k_f\right]\times\left[\left(\frac{\phi_{Al_2O_3}k_{Al_2O_3}+\phi_{Cu}k_{Cu}}{\phi_{hnf}}\right)+2k_f-(\phi_{Al_2O_3}k_{Al_2O_3}+\phi_{Cu}k_{Cu})+\phi_{hnf}k_f\right]^{-1},$$

$$\frac{\sigma_{hnf}}{\sigma_f}=\left[\left(\frac{\phi_{Al_2O_3}\sigma_{Al_2O_3}+\phi_{Cu}\sigma_{Cu}}{\phi_{hnf}}\right)+2\sigma_f+2(\phi_{Al_2O_3}\sigma_{Al_2O_3}+\phi_{Cu}\sigma_{Cu})-2\phi_{hnf}\sigma_f\right]\times\left[\left(\frac{\phi_{Al_2O_3}\sigma_{Al_2O_3}+\phi_{Cu}\sigma_{Cu}}{\phi_{hnf}}\right)+2\sigma_f-(\phi_{Al_2O_3}\sigma_{Al_2O_3}+\phi_{Cu}\sigma_{Cu})+\phi_{hnf}\sigma_f\right]^{-1}$$

$$\beta_{hnf}=\frac{1}{\rho_{hnf}}(\phi_{Al_2O_3}\rho_{Al_2O_3}\beta_{Al_2O_3}+\phi_{Cu}\rho_{Cu}\beta_{Cu}+(1-\phi_{hnf})\rho_f\beta_f)$$

These correlations are established in regards to the physical assumptions that are well agreed with the mass and energy conservations. The nanoparticle concentration volume parameter is symbolized as ϕ ($\phi=0$ is a regular fluid, $\phi_{Al_2O_3}=\phi_1$ is for alumina nanoparticle and $\phi_{Cu}=\phi_2$ is for copper nanoparticle), ρ is the density, k is the thermal conductivity, $(\rho C_p)$is the heat capacity, C_p is the specific heat with fixed pressure, σ is the electrical conductivity and β is the thermal expansion where the subscript of hnf, f, Al_2O_3 and Cu are referred to the hybrid nanofluid, base fluid, alumina nanoparticle, and copper nanoparticle, respectively. The thermophysical properties of the component in hybrid nanofluids are displayed in Table 1.

To simplify the governing equations, the following similarity variables are introduced towards the model [48,53,54]:

$$u=U_0f'(\eta),\ v=-\frac{1}{2x}\sqrt{xv_fU_0}[f(\eta)-\eta f'(\eta)],$$
$$\theta(\eta)=\frac{(T-T_\infty)}{(T_w-T_\infty)},\ \eta=y\sqrt{\frac{U_0}{xv_f}} \tag{8}$$

such that $v_w(x)$ can be expressed as

$$v_w(x)=-\frac{1}{2x}\sqrt{xU_0v_f}S \tag{9}$$

Table 1 Thermophysical properties (Oztop and Abu-Nada [52], Devi and Devi [5]).

Properties	Water	Alumina	Copper
$\rho\left(\mathrm{kg/m^3}\right)$	997.1	3970	8933
$C_p(\mathrm{J/kgK})$	4179	765	385
$k(\mathrm{W/mK})$	0.613	40	400
$\sigma(\mathrm{S/m})$	5.5×10^{-6}	35×10^{6}	59.6×10^{6}
$\beta(1/\mathrm{K})$	21×10^{-5}	0.85×10^{-5}	1.67×10^{-5}
Pr	6.2		

where the primes denote the differentiation of f and θ that regards to η, also U_0 is a velocity characteristic and S is the constant mass flux velocity with $S > 0$ for suction and $S < 0$ for injection, accordingly.

Using Eq. (8), Eqs. (2) and (6) are remodeled into the system of ODEs:

$$\frac{\mu_{hnf}/\mu_f}{\rho_{hnf}/\rho_f} f''' + \frac{1}{2} f f'' - \frac{\sigma_{hnf}/\sigma_f}{\rho_{hnf}/\rho_f} M f' + \frac{\beta_{hnf}}{\beta_f} \lambda\theta = 0 \tag{10}$$

$$\frac{1}{\mathrm{Pr}} \frac{(\rho C_p)_f}{(\rho C_p)_{hnf}} \left(\frac{k_{hnf}}{k_f} + \frac{4}{3} Rd\right) \theta'' + \frac{1}{2} f\theta' - f'\theta = 0 \tag{11}$$

together with the boundary conditions

$$\begin{gathered} f(0) = S,\ f'(0) = 0,\ -\tfrac{k_{hnf}}{k_f}\theta'(0) = Bi(1 - \theta(0)) \\ f'(\infty) \to 0,\ \theta(\infty) \to 0 \end{gathered} \tag{12}$$

Here, Pr is the Prandtl number, Rd is radiation parameter, Bi is the Biot number, M is the magnetic parameter, and λ is the mixed convection parameter where $\lambda > 0$ refers to the assisting flow, $\lambda < 0$ is for opposing flow, and $\lambda = 0$ is the forced convection flow. These parameters can be specifically expressed as

$$\begin{gathered} \mathrm{Pr} = \frac{(\nu\rho C_p)_f}{k_f},\ Rd = \frac{4\sigma^* T_\infty^3}{k^* k_f},\ Bi = \frac{\bar{h}_f}{k_f}\sqrt{\frac{\nu_f L}{U_0}},\ M = \frac{x\sigma_f B_0^2}{\rho_f U_0}, \\ \lambda = \frac{Gr_x}{Re_x^2} \end{gathered} \tag{13}$$

where $Re_x = U_0 x/\nu_f$ is the local Reynolds number and $Gr_x = g\beta_f(T_w - T_\infty)x^3/\nu_f^2$ is the local Grashof number.

The physical quantities of interest which are the skin friction coefficient C_f and the local Nusselt number Nu_x are written as

$$\begin{aligned} C_f &= \frac{\mu_{hnf}}{\rho_f U_0^2}\left(\frac{\partial u}{\partial y}\right)_{y=0},\ Nu_x \\ &= -\frac{x k_{hnf}}{k_f(T_w - T_\infty)}\left(\frac{\partial T}{\partial y}\right)_{y=0} + \frac{x}{k_f(T_w - T_\infty)}(q_r)_{y=0} \end{aligned} \tag{14}$$

Implementing Eq. (8), Eq. (14) is simplified into

$$Re_x^{1/2} C_f = \frac{\mu_{hnf}}{\mu_f} f''(0),\ Re_x^{-1/2} Nu_x = -\left(\frac{k_{hnf}}{k_f} + \frac{4}{3} Rd\right)\theta'(0) \tag{15}$$

3. Stability analysis

The nature of the system in Eqs. (10) and (11) connote that for a specific range of the mixed convection parameter λ, more than one numerical solution can be revealed. Ergo, the analysis of stability is needed to identify which of the solution is stable (see Merkin [55] and Weidman et al. [56]). With that being said, the introduction of new similarity variables for the transformation are required, which are specified as

$$\begin{gathered} u = U_0 \tfrac{\partial f}{\partial \eta}(\eta,\tau),\ v = -\tfrac{1}{2x}\sqrt{x\nu_f U_0}\left[f(\eta,\tau) - \eta\tfrac{\partial f}{\partial \eta}(\eta,\tau)\right], \\ \theta(\eta,\tau) = \tfrac{(T - T_\infty)}{(T_w - T_\infty)},\ \eta = y\sqrt{\tfrac{U_0}{x\nu_f}},\ \tau = \tfrac{U_0 t}{x} \end{gathered} \tag{16}$$

where τ is the dimensionless time variable and t is time. Substitute Eq. (16) into Eqs. (2) and (6) that are set to be unsteady, the subsequent equations can be attained

$$\frac{\mu_{hnf}/\mu_f}{\rho_{hnf}/\rho_f}\frac{\partial^3 f}{\partial \eta^3} + \frac{1}{2} f\frac{\partial^2 f}{\partial \eta^2} - \frac{\sigma_{hnf}/\sigma_f}{\rho_{hnf}/\rho_f} M\frac{\partial f}{\partial \eta} + \frac{\beta_{hnf}}{\beta_f}\lambda\theta - \frac{\partial^2 f}{\partial \eta \partial \tau} = 0 \tag{17}$$

$$\frac{1}{\mathrm{Pr}}\frac{(\rho C_p)_f}{(\rho C_p)_{hnf}}\left(\frac{k_{hnf}}{k_f} + \frac{4}{3} Rd\right)\frac{\partial^2 \theta}{\partial \eta^2} + \frac{1}{2} f\frac{\partial \theta}{\partial \eta} - \frac{\partial f}{\partial \eta}\theta - \frac{\partial \theta}{\partial \tau} = 0 \tag{18}$$

alongside the boundary conditions

$$\begin{gathered} f(0,\tau) = S,\ \tfrac{\partial f}{\partial \eta}(0,\tau) = 0,\ -\tfrac{k_{hnf}}{k_f}\tfrac{\partial \theta}{\partial \eta}(0,\tau) = Bi(1 - \theta(0,\tau)) \\ \tfrac{\partial f}{\partial \eta}(\infty,\tau) \to 0,\ \theta(\infty,\tau) \to 0 \end{gathered} \tag{19}$$

To test the steady flow stability $f(\eta) = f_0(\eta)$ and $\theta(\eta) = \theta_0(\eta)$ fulfilling the boundary value problem Eqs. (10)–(12), we implement the perturbed equations such that

$$\begin{aligned} f(\eta,\tau) &= f_0(\eta) + e^{-\gamma\tau}F(\eta), \\ \theta(\eta,\tau) &= \theta_0(\eta) + e^{-\gamma\tau}G(\eta), \end{aligned} \tag{20}$$

where γ is the eigenvalue parameter and functions $F(\eta)$ and $G(\eta)$ are the small relative to $f_0(\eta)$ and $\theta_0(\eta)$. Inserting Eq. (20) into Eqs. (17)–(19), fixing $\tau \to 0$ and simplifying the equations, the following linearized eigenvalue problem is developed

$$\frac{\mu_{hnf}/\mu_f}{\rho_{hnf}/\rho_f}F''' + \frac{1}{2}\left(f_0 F'' + F f_0''\right) - \frac{\sigma_{hnf}/\sigma_f}{\rho_{hnf}/\rho_f} M F' + \frac{\beta_{hnf}}{\beta_f}\lambda G + \gamma F' = 0 \tag{21}$$

$$\begin{aligned} &\frac{1}{\mathrm{Pr}}\frac{(\rho C_p)_f}{(\rho C_p)_{hnf}}\left(\frac{k_{hnf}}{k_f} + \frac{4}{3} Rd\right)G'' + \frac{1}{2}\left(f_0 G' + F\theta_0'\right) \\ &\quad - \left(f_0' G + F'\theta_0\right) + \gamma G = 0 \end{aligned} \tag{22}$$

followed by the conditions

$$\begin{gathered} F(0) = 0,\ F'(0) = 0,\ \tfrac{k_{hnf}}{k_f}G'(0) = BiG(0), \\ F'(\infty) \to 0,\ G(\infty) \to 0. \end{gathered} \tag{23}$$

Before solving the linearized eigenvalue problem, the boundary conditions that are specified in Eq. (23) need to be adjusted. Harris et al. [57] suggested that one of the far-field boundary condition needs to be relaxed and replaced (see also Tadesse et al. [58], Tshivhi and Makinde [59]). So, in this study, it is impossible to relax $G(\infty) \to 0$ because it will be replaced with $G'(0) = 1$ which somehow will affect the other boundary conditions and affect the numerical solutions. Hence, we chose $F'(\infty) \to 0$ to be relaxed and replaced with $F''(0) = 1$.

As solving Eqs. (21) and (22) together with the adjusted boundary conditions, it is noticed that the solutions produce an infinite set of eigenvalues $\gamma_1 < \gamma_2 < \gamma_3 ...$, where γ_1 attributes to the minimum eigenvalue. From this, the stability of the solution can be identified where, $\gamma_1 > 0$ indicates the solution to be stable, whilst $\gamma_1 < 0$ indicates the solution to be unstable due to the growth of the disturbance of the solution.

4. Numerical procedure and validation

The ODEs (see Eqs. (10)–(11)) with the boundary conditions Eq. (12) are evaluated with the facilitation of a numerical solver known as bvp4c (MATLAB). This solver follows the finite difference scheme programmed with three-stage Lobatto IIIa formula which is a collocation formula that provides the fourth-order accuracy. Before importing the model into the solver, Eqs. (10)–(12) should be readjusted in the following form of codes:

$$f = y(1),\ f' = y(2),\ f'' = y(3),\ \theta = y(4),\ \theta' = y(5) \tag{24}$$

$$\begin{aligned} f''' &= \frac{1}{\frac{\mu_{hnf}/\mu_f}{\rho_{hnf}/\rho_f}}\left(-\tfrac{1}{2}ff'' + \frac{\sigma_{hnf}/\sigma_f}{\rho_{hnf}/\rho_f}Mf' - \frac{\beta_{hnf}}{\beta_f}\lambda\theta\right) \\ &= \frac{1}{\frac{\mu_{hnf}/\mu_f}{\rho_{hnf}/\rho_f}}\left(-\tfrac{1}{2}y(1)y(3)f'' + \frac{\sigma_{hnf}/\sigma_f}{\rho_{hnf}/\rho_f}My(2) - \frac{\beta_{hnf}}{\beta_f}\lambda y(4)\right) \end{aligned} \tag{25}$$

$$\begin{aligned} \theta'' &= \frac{1}{\frac{1}{\Pr}\frac{(\rho C_p)_f}{(\rho C_p)_{hnf}}\left(\frac{k_{hnf}}{k_f} + \frac{4}{3}Rd\right)}\left(-\tfrac{1}{2}f\theta' + f'\theta\right) \\ &= \frac{1}{\frac{1}{\Pr}\frac{(\rho C_p)_f}{(\rho C_p)_{hnf}}\left(\frac{k_{hnf}}{k_f} + \frac{4}{3}Rd\right)}\left(-\tfrac{1}{2}y(1)y(5) + y(2)y(4)\right) \end{aligned} \tag{26}$$

$$\begin{aligned} &ya(1) - S,\ ya(2),\ -\frac{k_{hnf}}{k_f}ya(5) \\ &\quad - Bi(1 - ya(4)),\ yb(2),\ yb(4) \end{aligned} \tag{27}$$

Here, ya and yb is the boundary conditions when $\eta = 0$ and $\eta \to \infty$, respectively. The suitable boundary layer thickness, the initial guesses, and the value of the parameter should be set accordingly to execute the acceptable solution. The numerical solution is found to be acceptable when there is no warning or error produced during the execution, and the far-field boundary conditions are met. It is common to note that the first (upper branch) solution is the stable solution when there exists more than one solution. In this case, stability analysis should be conducted to validate the stability of the solution as has been briefly explained in the previous section. Thus, to solve and analyze the stability of the flow, Eqs. (21) and (22) with the boundary conditions Eq. (23) that consider the appropriate relaxation, should be modified to the following form to be solved in the solver program:

$$F = y(1),\ F' = y(2),\ F'' = y(3),\ G = y(4),\ G' = y(5) \tag{28}$$

$$f_0 = s(1),\ f_0' = s(2),\ f_0'' = s(3), \theta_0 = s(4),\ \theta_0' = s(5) \tag{29}$$

$$\begin{aligned} F''' &= \frac{1}{\frac{\mu_{hnf}/\mu_f}{\rho_{hnf}/\rho_f}}\left(-\tfrac{1}{2}\left(f_0F'' + Ff_0''\right) + \frac{\sigma_{hnf}/\sigma_f}{\rho_{hnf}/\rho_f}MF' - \frac{\beta_{hnf}}{\beta_f}\lambda G - \gamma F'\right) \\ &= \frac{1}{\frac{\mu_{hnf}/\mu_f}{\rho_{hnf}/\rho_f}}\left(-\tfrac{1}{2}(s(1)y(3) + y(1)s(3)) + \frac{\sigma_{hnf}/\sigma_f}{\rho_{hnf}/\rho_f}My(2) - \frac{\beta_{hnf}}{\beta_f}\lambda y(4) - \gamma y(2)\right) \end{aligned} \tag{30}$$

$$\begin{aligned} G'' &= \frac{1}{\frac{1}{\Pr}\frac{(\rho C_p)_f}{(\rho C_p)_{hnf}}\left(\frac{k_{hnf}}{k_f} + \frac{4}{3}Rd\right)}\left(-\tfrac{1}{2}\left(f_0G' + F\theta_0'\right) + \left(f_0'G + F'\theta_0\right) - \gamma G\right) \\ &= \frac{\Pr\frac{(\rho C_p)_{hnf}}{(\rho C_p)_f}}{\left(\frac{k_{hnf}}{k_f} + \frac{4}{3}Rd\right)}\left(-\tfrac{1}{2}\left(s(1)y(5) + y(1)s(5)\right) + \left(s(2)y(4) + y(2)s(4)\right) - \gamma y(4)\right) \end{aligned} \tag{31}$$

$$ya(1) - S,\ ya(2),\ \frac{k_{hnf}}{k_f}ya(5) - Bi\ ya(4), ya(3) - 1, yb(4) \tag{32}$$

For the validation, we make a comparison towards the values of $f''(0)$ when $M = \lambda = 0$ and $\phi_{Al2O3} = \phi_{Cu} \approx 0$ with the previous studies as can be seen in Table 2. The data are noticeable to be well agreed and consequently validate the model formulation, numerical computation, and the executed results. Only for the validation and comparison purpose, it should be noted here, this comparison is made when one of the far-field boundary conditions is set to be $f'(\infty) \to 1$ which is slightly different from the presented conditions provided initially in this study (the condition is set to be $f'(\infty) \to 0$). The study presented by Mukhopadhyay and Chandra Mandal [54], Bhattacharyya and Layek [53], as well as Howarth and Bairstow [60], are the most comparable study that are available for the validation purpose as a similar model is hard to be found. However, this somehow also could confirm that the model and results provided in this present study are still new and original.

5. Results and discussion

To achieve the understanding towards the effect of various parameters considered in the model such as the (copper) concentration volume ϕ_2, magnetic M, radiation Rd, Biot number Bi and mixed convection parameter λ towards the flow and heat transfer properties; the skin friction coefficient $Re_x^{1/2}C_f$, the local Nusselt number $Re_x^{-1/2}Nu_x$ as well as the velocity

Table 2 Skin friction coefficient when $M = \lambda = 0$ and $\phi_{Al_2O_3} = \phi_{Cu} \approx 0$.

$f''(0)$			
Present	Mukhopadhyay and Chandra Mandal [54]	Bhattacharyya and Layek [53]	Howarth and Bairstow [60]
0.332057347	0.332058	0.332058	0.33206

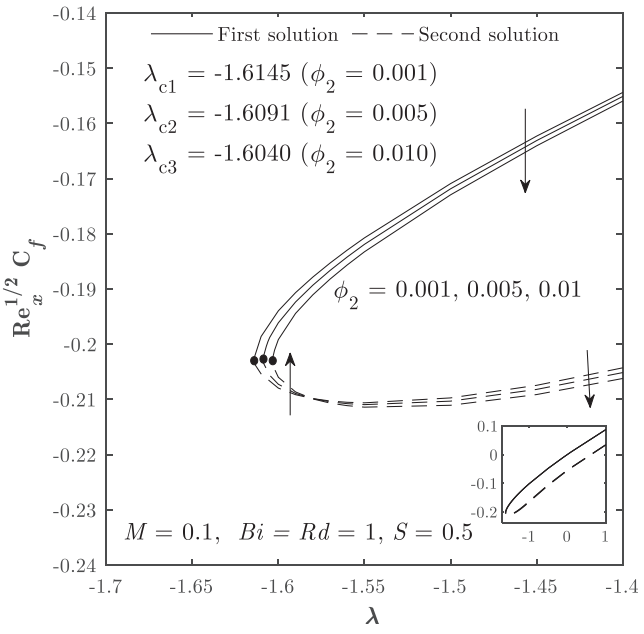

Fig. 2 $Re_x^{1/2}C_f$ against λ with changing ϕ_2.

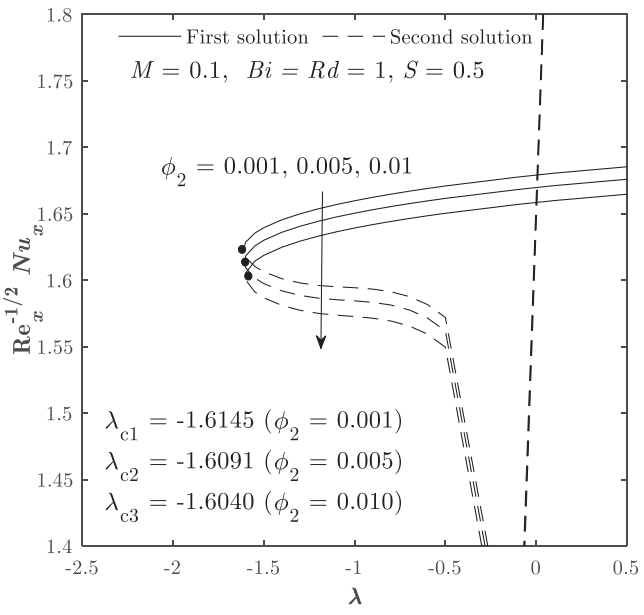

Fig. 3 $Re_x^{-1/2}Nu_x$ against λ with changing ϕ_2.

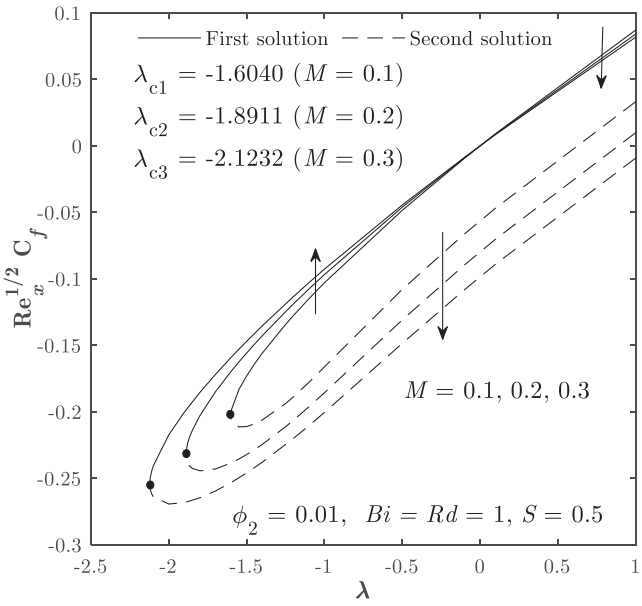

Fig. 4 $Re_x^{1/2}C_f$ against λ with changing M.

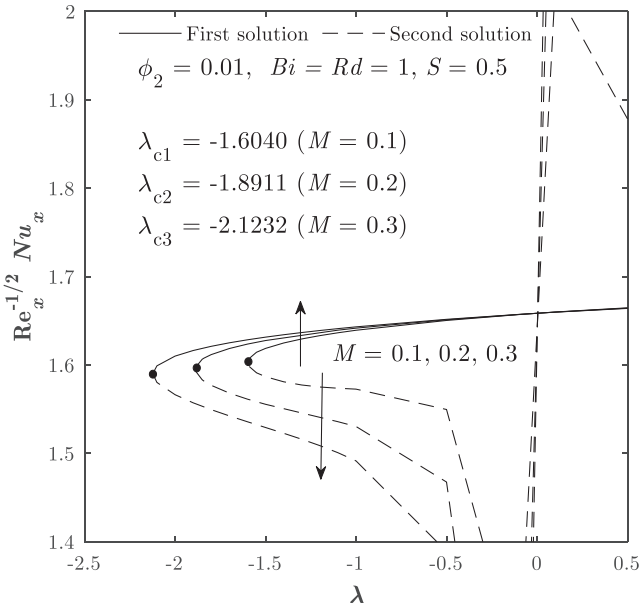

Fig. 5 $Re_x^{-1/2}Nu_x$ against λ with changing M.

$f'(\eta)$ and temperature $\theta(\eta)$ profiles are illustrated in the form of graph (see Figs. 2-11). Several findings can be extracted through the observation from the graphical illustration such as (i) the relation between the effects and the physical quantities, (ii) the determination of parameters that affect the boundary separation, and (iii) the factor that causes the dual solutions to be visible. It should be mentioned here that we have fixed the concentration volume for alumina (ϕ_1) to be 1% throughout the study, meanwhile, the concentration volume for copper (ϕ_2) is set to be varied between 0.1% until 1%. For future reference, we also provide the numerical solutions for $Re_x^{1/2}C_f$ and $Re_x^{-1/2}Nu_x$ in data tabulation as in Tables 3 and 4.

Figs. 2 and 3 display the variation of $Re_x^{1/2}C_f$ and $Re_x^{-1/2}Nu_x$ against λ with the changing ϕ_2, respectively. The critical point is seen to be visible at the opposing flow ($\lambda < 0$) of the mixed convection parameter which indicates that this parameter causes the dual solutions to be established. Besides, the boundary layer separation can be impeded with the decrement of ϕ_2. This critical point is the indicator point for the separation of the boundary layer from laminar to turbulent flow. From Fig. 2, it is observable that the incrementation of ϕ_2 can reduce the value of $Re_x^{1/2}C_f$ for the first solution. However, for the second solution, there is inconsistent behavior of $Re_x^{1/2}C_f$ for changing ϕ_2 as the value of λ is moving. The value of $Re_x^{1/2}C_f$ is also seen to increase as the value of λ increase.

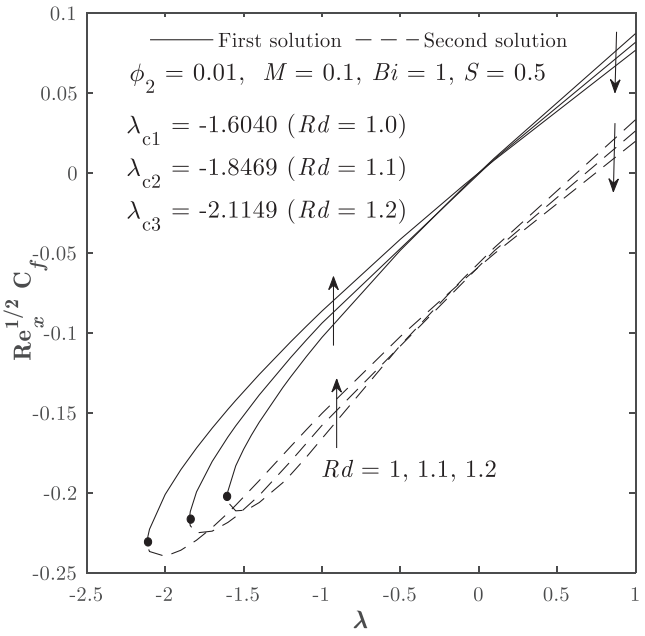

Fig. 6 $Re_x^{1/2}C_f$ against λ with changing Rd.

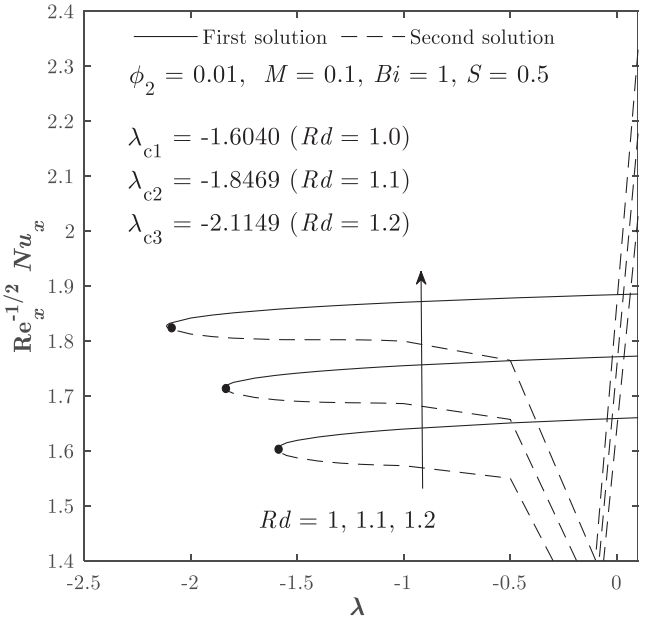

Fig. 7 $Re_x^{-1/2}Nu_x$ against λ with changing Rd.

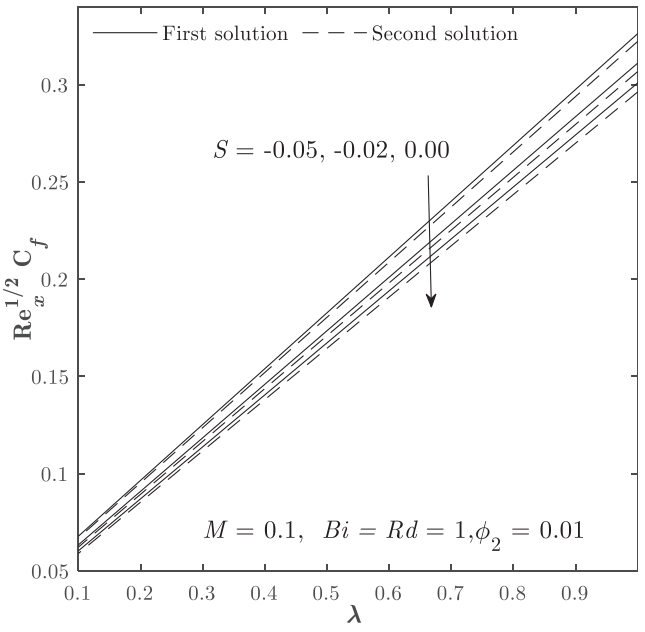

Fig. 8 $Re_x^{1/2}C_f$ against λ with changing S.

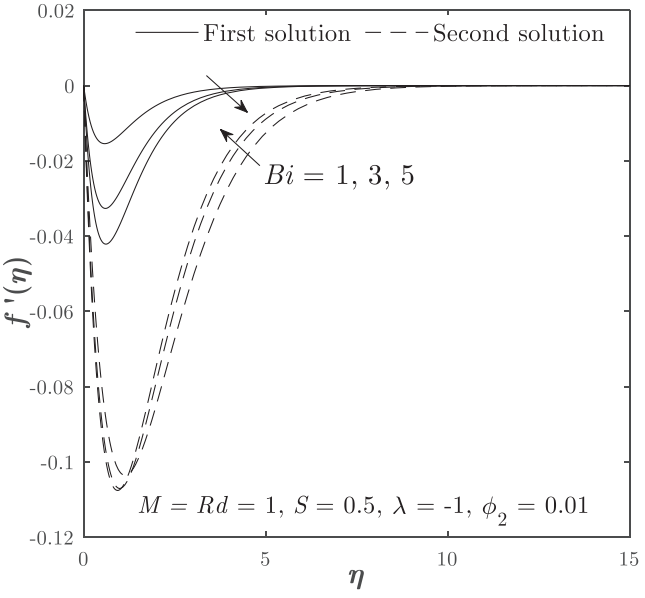

Fig. 9 $f'(\eta)$ with changing Bi.

Meanwhile, from Fig. 3, the incrementation of ϕ_2 for the first solution able to reduce $Re_x^{-1/2}Nu_x$ and the same pattern is also seen for the second solution.

Figs. 4 and 5 depict the variation of $Re_x^{1/2}C_f$ and $Re_x^{-1/2}Nu_x$ against λ with the changing M, respectively. The critical point is also noticed to be located at $\lambda < 0$. The proliferation of M helps to slow down the separation of the boundary layer and the incrementation of M causes an enhancement for $Re_x^{1/2}C_f$ at $\lambda < 0$, and reduction for $Re_x^{1/2}C_f$ at $\lambda > 0$, for the first solution. Meanwhile, for the second solution, the increment of M also reduces the value of $Re_x^{1/2}C_f$ for both opposing and assisting flow of mixed convection. Besides, the value of $Re_x^{-1/2}Nu_x$ can be increased when M is augmented for the first solution and otherwise for the other solution.

Moreover, Figs. 6 and 7 reveal the variation of $Re_x^{1/2}C_f$ and $Re_x^{-1/2}Nu_x$ against λ with the changing Rd, respectively. The enhancement of Rd aids in hindering the separation of the boundary layer, whilst the critical point that becomes the starting point of the flow separation eventuates at $\lambda < 0$. Similar to the previous figure, the augmentation of Rd increases the value of $Re_x^{1/2}C_f$ when $\lambda < 0$, and decreases the value of $Re_x^{1/2}C_f$ when $\lambda > 0$, for the first solution. A similar manner is also observable for the second solution. Meanwhile, the incremen-

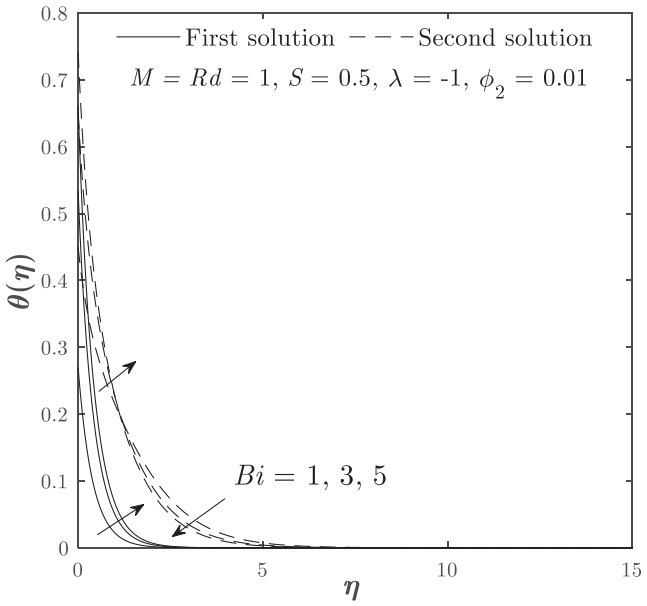

Fig. 10 $\theta(\eta)$ with changing *Bi*.

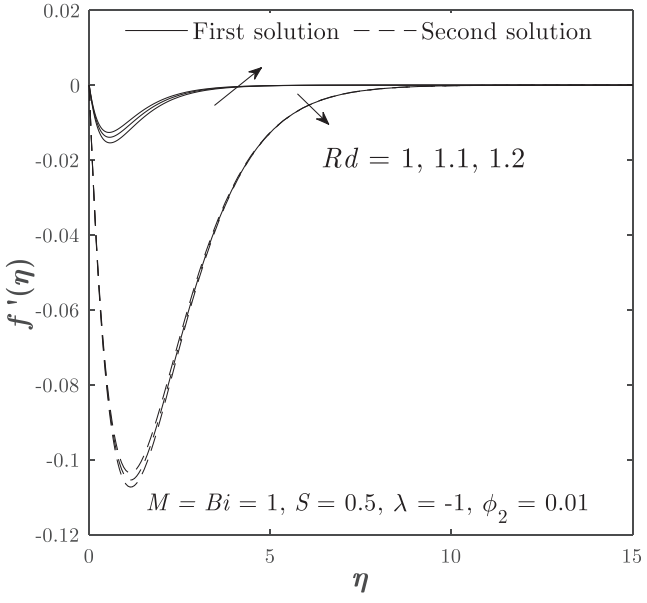

Fig. 11 $f'(\eta)$ with changing *Rd*.

tation of *Rd* increases the value of $Re_x^{-1/2}Nu_x$ for both first and second solutions.

Fig. 8 displays the variation of $Re_x^{1/2}C_f$ against λ with the changing S, in which for injection ($S < 0$) and impermeable ($S = 0$) plate. Unlike for the case of suction ($S > 0$), in this case of injection and impermeable plate, the variation of $Re_x^{1/2}C_f$ is seen to only feasible when $\lambda > 0$. However, fortunately, dual solutions are still visible within this range because of the opposing flow provided by injection, but no critical value is found. According to the figure too, the intensification of S (reduction of injection from -0.05 to 0) is noted to decrease the value of $Re_x^{1/2}C_f$, where the incrementation of 3% of S can reduce the skin friction by approximately 0.016–0.045% within ($0 < \lambda < 1$). Nonetheless, $Re_x^{1/2}C_f = 0$ when $\lambda = 0$ regardless the value of S.

Figs. 9-12 exemplify the velocity and temperature profiles for changing *Bi* and *Rd* when $\lambda = -1$. The effect of *Bi* and *Rd* will not affect the velocity profile if $\lambda = 0$ and only just affect the temperature profile. As can be observed from the figures, the increment of *Bi* for the first solution causes the velocity profile to deplete and causes the temperature profile to increase. Nevertheless, the opposite manner has occurred for the first solution of *Rd* when compared to the pattern of *Bi*. Physically, as more *Rd* is considered, more heat also is radiated towards the model which then causes the temperature to increase.

As dual solutions are observed to be visible in the findings, we also have conducted the stability analysis to determine the practicality of the solution. From the analysis, it can be summarized that only the first solution is considered as the stable and practical solution for the guidance in the real application. This claim is supported through the tabulation and graphical representation as can be seen in Table 5 and Fig. 13, where the solution is noted to be stable when the executed minimum eigenvalues are positive and otherwise for the non-stable solution. From Fig. 13 also, we can note that as λ goes towards its critical value, then the smallest eigenvalue will tend to zero, which is true to verify the results obtained through the stability analysis and validates the claim that the first solution is stable.

6. Conclusion

MHD radiative flow of a hybrid nanofluid past a permeable vertical flat plate with mixed convection has been successfully scrutinized with the facilitation of bvp4c solver. The dual solutions are achievable due to the opposing flow of the mixed convection parameter with the combination of appropriate

Table 3 Tabulation $Re_x^{1/2}C_f$ when $Bi = 1$, $S = 2.5$, Pr = 6.2 and $\lambda = -1$.

ϕ_1	ϕ_2	M	Rd	$Re_x^{1/2}C_f$	
				First solution	Second solution
0	0	0.1	1.0	−0.068592722	−0.946637258
0.01	0.001			−0.068313307	−0.976577448
	0.005			−0.068335402	−1.005161920
	0.010			−0.068366703	−1.040991185

Table 4 Tabulation $Re_x^{-1/2}Nu_x$ when $Bi = 1$, $S = 2.5$, Pr = 6.2 and $\lambda = -1$.

ϕ_1	ϕ_2	M	Rd	$Re_x^{-1/2}Nu_x$	
				First solution	Second solution
0	0	0.1	1.0	1.792270390	1.209004905
0.01	0.001			1.766220882	1.167873050
	0.005			1.756660336	1.142322221
	0.010			1.745156143	1.110804812

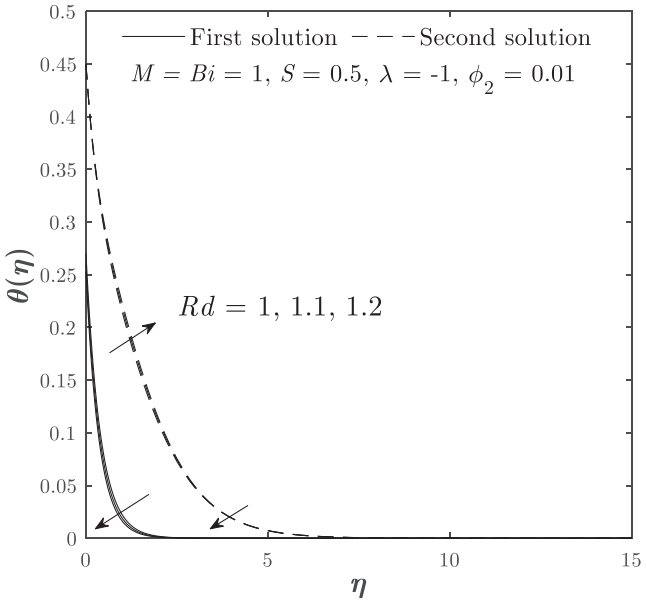

Fig. 12 $\theta(\eta)$ with changing Rd.

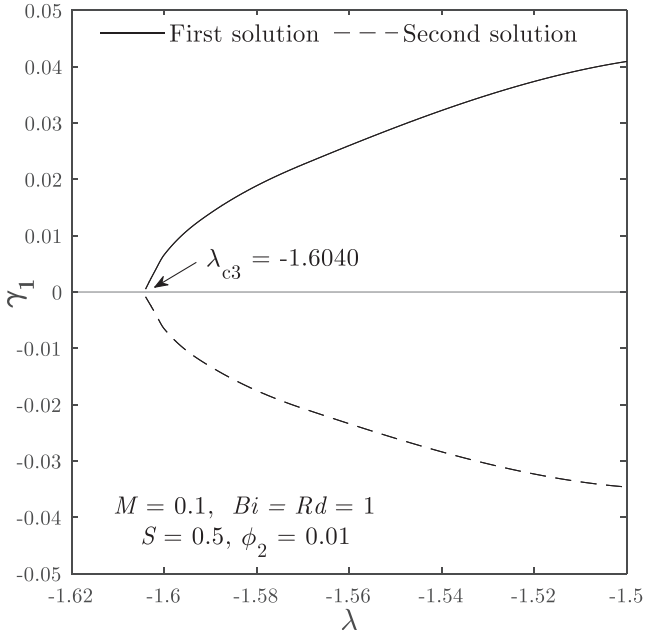

Fig. 13 γ_1 against λ.

Table 5 Variation of minimum eigenvalue γ_1 for selected λ when $M = 0.1$, $Bi = Rd = 1$, $S = 0.5$ and $\phi_{Al_2O_3} = 0.01$.

λ	γ_1	
	First solution	Second solution
−1.6040	0.00052	−0.00085
−1.6020	0.00370	−0.00365
−1.6000	0.00659	−0.00651
−1.5000	0.04094	−0.03462

amount of the other parameters. The first solution presented in this study is the stable solution and otherwise for another solution. In this work, the incrementation of concentration volume of copper is noted to accelerate the boundary layer separation and reduce the physical quantities of interest. The mixed convection parameter is overall enhancing the skin friction and the heat transfer rate specifically for the realizable solution. The numerical solutions presented in this study can be further used as a reference and guidance to authenticate the validity of numerical solutions from other related mixed convection problems.

Declaration of Competing Interest

The authors declare that they have no known competing financial interests or personal relationships that could have appeared to influence the work reported in this paper.

Acknowledgement

The financial support through the Fundamental Research Grant Scheme (KPTFRGS/1/2019/STG06/IPM/02/3, Vot 5540309) from Ministry of Higher Education (Malaysia) is appreciatively acknowledged including the support from Universiti Putra Malaysia and Universiti Teknikal Malaysia Melaka.

References

[1] S.U.S. Choi, J.A. Eastman, Enhancing thermal conductivity of fluids with nanoparticles, ASME Fluids Eng. Div. 231 (1995) 99–106.

[2] M. Muneeshwaran, G. Srinivasan, P. Muthukumar, C.-C. Wang, Role of hybrid-nanofluid in heat transfer enhancement – A review, Int. Commun. Heat Mass Transf. 125 (2021) 105341, https://doi.org/10.1016/j.icheatmasstransfer.2021.105341.

[3] F. Jamil, H.M. Ali, Applications of hybrid nanofluids in different fields, in: Hybrid Nanofluids Convect. Heat Transf., Elsevier, 2020: pp. 215–254. http://doi.org/10.1016/B978-0-12-819280-1.00006-9.
[4] D.P. Kshirsagar, M.A. Venkatesh, A review on hybrid nanofluids for engineering applications, Mater. Today Proc. 44 (2021) 744–755, https://doi.org/10.1016/j.matpr.2020.10.637.
[5] S.P.A. Devi, S.S.U. Devi, Numerical Investigation of Hydromagnetic Hybrid Cu –Al_2O_3/Water Nanofluid Flow over a Permeable Stretching Sheet with Suction, Int. J. Nonlinear Sci. Numer. Simul. 17 (2016) 249–257, https://doi.org/10.1515/ijnsns-2016-0037.
[6] S.U. Devi, S.A. Devi, Heat transfer enhancement of Cu-Al_2O_3/water hybrid nanofluid flow over a stretching sheet, J. Nigerian Mathem. Soc. 36 (2017) 419–433.
[7] B. Takabi, S. Salehi, Augmentation of the Heat Transfer Performance of a Sinusoidal Corrugated Enclosure by Employing Hybrid Nanofluid, Adv. Mech. Eng. 6 (2014) 147059, https://doi.org/10.1155/2014/147059.
[8] A.T. Olatundun, O.D. Makinde, Analysis of Blasius Flow of Hybrid Nanofluids over a Convectively Heated Surface, Defect Diffus. Forum. 377 (2017) 29–41, https://doi.org/10.4028/www.scientific.net/DDF.377.29.
[9] R.I. Yahaya, N.M. Arifin, R. Nazar, I. Pop, Flow and heat transfer past a permeable stretching/shrinking sheet in Cu−Al $_2$ $_O$ *3* / water hybrid nanofluid, Int. J. Numer. Methods Heat Fluid Flow. 30 (3) (2019) 1197–1222, https://doi.org/10.1108/HFF-05-2019-0441.
[10] P. Sreedevi, P. Sudarsana Reddy, A. Chamkha, Heat and mass transfer analysis of unsteady hybrid nanofluid flow over a stretching sheet with thermal radiation, SN, Appl. Sci. 2 (7) (2020), https://doi.org/10.1007/s42452-020-3011-x.
[11] R. Jusoh, K. Naganthran, A. Jamaludin, M.H. Ariff, M.F.M. Basir, I. Pop, Mathematical analysis of the flow and heat transfer of Ag-Cu hybrid nanofluid over a stretching/shrinking surface with convective boundary condition and viscous dissipation, Data Anal. Appl. Math. DAAM. 1 (2020) 11–22, https://doi.org/10.15282/daam.v1i01.5105.
[12] N.S. Khashi'ie, N. Md Arifin, I. Pop, R. Nazar, Melting heat transfer in hybrid nanofluid flow along a moving surface, J. Therm. Anal. Calorim. (2020). http://doi.org/10.1007/s10973-020-10238-4.
[13] N.S. Khashi'ie, N. Md Arifin, I. Pop, R. Nazar, E.H. Hafidzuddin, N. Wahi, Thermal Marangoni Flow Past a Permeable Stretching/Shrinking Sheet in a Hybrid Cu-Al2O3/Water Nanofluid, Sains Malays. 49 (1) (2020) 211–222, https://doi.org/10.17576/jsm10.17576/jsm-2020-490110.17576/jsm-2020-4901-25.
[14] N.S. Khashi'ie, E.H. Hafidzuddin, N.M. Arifin, N. Wahi, Stagnation Point Flow of Hybrid Nanofluid over a Permeable Vertical Stretching/Shrinking Cylinder with Thermal Stratification Effect, CFD Lett. 12 (2020) 80–94.
[15] Najiyah S. Khashiie, Norihan M. Arifin, Ioan Pop, Nur S. Wahid, Effect of suction on the stagnation point flow of hybrid nanofluid toward a permeable and vertical Riga plate, Heat Transf. 50 (2) (2021) 1895–1910, https://doi.org/10.1002/htj.v50.210.1002/htj.21961.
[16] Nur Syazana Anuar, Norfifah Bachok, Norihan Md Arifin, Haliza Rosali, Analysis of Al_2O_3-Cu nanofluid flow behaviour over a permeable moving wedge with convective surface boundary conditions, J. King Saud Univ. - Sci. 33 (3) (2021) 101370, https://doi.org/10.1016/j.jksus.2021.101370.
[17] Sayer Obaid Alharbi, Influence of wall slip and jump in wall temperature on transport of heat energy in hybrid nanofluid, J. Therm. Anal. Calorim. 144 (3) (2021) 847–854, https://doi.org/10.1007/s10973-020-09428-x.
[18] Shahirah Abu Bakar, Norihan Md Arifin, Najiyah Safwa Khashi'ie, Norfifah Bachok, Hybrid Nanofluid Flow over a Permeable Shrinking Sheet Embedded in a Porous Medium with Radiation and Slip Impacts, Mathematics. 9 (8) (2021) 878, https://doi.org/10.3390/math9080878.
[19] Nur Syahirah Wahid, Norihan Md Arifin, Najiyah Safwa Khashi'ie, Ioan Pop, Marangoni hybrid nanofluid flow over a permeable infinite disk embedded in a porous medium, Int. Commun. Heat Mass Transf. 126 (2021) 105421, https://doi.org/10.1016/j.icheatmasstransfer.2021.105421.
[20] M.K. Nayak, V.S. Pandey, S. Shaw, O.D. Makinde, K.M. Ramadan, Mouna Ben Henda, Iskander Tlili, Thermo-fluidic significance of non Newtonian fluid with hybrid nanostructures, Case Stud, Therm. Eng. 26 (2021) 101092, https://doi.org/10.1016/j.csite.2021.101092.
[21] Najiyah Safwa Khashi'ie, Iskandar Waini, Nurul Amira Zainal, Khairum Hamzah, Abdul Rahman Mohd Kasim, Hybrid Nanofluid Flow Past a Shrinking Cylinder with Prescribed Surface Heat Flux, Symmetry. 12 (9) (2020) 493, https://doi.org/10.3390/sym12091493.
[22] Nur Syahirah Wahid, Norihan Md Arifin, Najiyah Safwa Khashi'ie, Ioan Pop, Hybrid Nanofluid Slip Flow over an Exponentially Stretching/Shrinking Permeable Sheet with Heat Generation, Mathematics. 9 (1) (2021) 30, https://doi.org/10.3390/math9010030.
[23] Nur Syahirah Wahid, Norihan Md Arifin, Najiyah Safwa Khashi'ie, Ioan Pop, Norfifah Bachok, Mohd Ezad Hafidz Hafidzuddin, Flow and heat transfer of hybrid nanofluid induced by an exponentially stretching/shrinking curved surface, Case Stud, Therm. Eng. 25 (2021) 100982, https://doi.org/10.1016/j.csite.2021.100982.
[24] Iskandar Waini, Anuar Ishak, Ioan Pop, Agrawal flow of a hybrid nanofluid over a shrinking disk, Case Stud. Therm. Eng. 25 (2021) 100950, https://doi.org/10.1016/j.csite.2021.100950.
[25] Najiyah Safwa Khashi'ie, Norihan Md Arifin, Ioan Pop, Roslinda Nazar, Dual solutions of bioconvection hybrid nanofluid flow due to gyrotactic microorganisms towards a vertical plate, Chin. J. Phys. 72 (2021) 461–474, https://doi.org/10.1016/j.cjph.2021.05.011.
[26] S. Das, R.N. Jana, O.D. Makinde, MHD Flow of Cu-Al_2O_3/Water Hybrid Nanofluid in Porous Channel: Analysis of Entropy Generation, Defect Diffus. Forum. 377 (2017) 42–61, https://doi.org/10.4028/www.scientific.net/DDF.377.42.
[27] N.S. Wahid, N. Md Arifin, M. Turkyilmazoglu, M.E.H. Hafidzuddin, N.A. Abd Rahmin, MHD Hybrid Cu-Al_2O_3/Water Nanofluid Flow with Thermal Radiation and Partial Slip Past a Permeable Stretching Surface. Analytical Solution, J. Nano Res. 64 (2020) 75–91, https://doi.org/10.4028/www.scientific.net/JNanoR.64.75.
[28] Mohammad Ghalambaz, Seyed Mohsen Hashem Zadeh, S.A. M. Mehryan, Ioan Pop, Dongsheng Wen, Analysis of melting behavior of PCMs in a cavity subject to a non-uniform magnetic field using a moving grid technique, Appl. Math. Model. 77 (2020) 1936–1953, https://doi.org/10.1016/j.apm.2019.09.015.
[29] N. Abbas, S. Nadeem, A. Saleem, M.Y. Malik, A. Issakhov, F. M. Alharbi, Models base study of inclined MHD of hybrid nanofluid flow over nonlinear stretching cylinder, Chin. J. Phys. 69 (2021) 109–117, https://doi.org/10.1016/j.cjph.2020.11.019.
[30] Faris Alzahrani, M. Ijaz Khan, Significance of induced magnetic force bio-convective flow of radiative Maxwell nanofluid with activation energy, Case Stud. Therm. Eng. 27 (2021) 101282, https://doi.org/10.1016/j.csite.2021.101282.
[31] N.S. Khashi'ie, I. Waini, N.M. Ari, I. Pop, Unsteady squeezing flow of Cu-Al2O3/water hybrid nanofluid in a horizontal channel with magnetic field, (2021). http://doi.org/10.21203/rs.3.rs-489942/v1.
[32] N.A. Zainal, R. Nazar, K. Naganthran, I. Pop, Heat generation/absorption effect on MHD flow of hybrid nanofluid over bidirectional exponential stretching/shrinking sheet, Chin. J.

Phys. 69 (2021) 118–133, https://doi.org/10.1016/j.cjph.2020.12.002.
[33] Mohammad Ghalambaz, S.A.M Mehryan, Nemat Mashoofi, Ahmad Hajjar, Ali J. Chamkha, Mikhail Sheremet, Obai Younis, Free convective melting-solidification heat transfer of nano-encapsulated phase change particles suspensions inside a coaxial pipe, Adv. Powder Technol. 31 (11) (2020) 4470–4481, https://doi.org/10.1016/j.apt.2020.09.022.
[34] M. Ghalambaz, A.J. Chamkha, D. Wen, Natural convective flow and heat transfer of Nano-Encapsulated Phase Change Materials (NEPCMs) in a cavity, Int. J. Heat Mass Transf. 138 (2019) 738–749, https://doi.org/10.1016/j.ijheatmasstransfer.2019.04.037.
[35] Mohammad Ghalambaz, S.A.M. Mehryan, Iman Zahmatkesh, Ali Chamkha, Free convection heat transfer analysis of a suspension of nano–encapsulated phase change materials (NEPCMs) in an inclined porous cavity, Int. J. Therm. Sci. 157 (2020) 106503, https://doi.org/10.1016/j.ijthermalsci.2020.106503.
[36] C.J. Ho, Yen-Chung Liu, Mohammad Ghalambaz, Wei-Mon Yan, Forced convection heat transfer of Nano-Encapsulated Phase Change Material (NEPCM) suspension in a mini-channel heatsink, Int. J. Heat Mass Transf. 155 (2020) 119858, https://doi.org/10.1016/j.ijheatmasstransfer.2020.119858.
[37] Iskandar Waini, Anuar Ishak, Teodor Groşan, Ioan Pop, Mixed convection of a hybrid nanofluid flow along a vertical surface embedded in a porous medium, Int. Commun. Heat Mass Transf. 114 (2020) 104565, https://doi.org/10.1016/j.icheatmasstransfer.2020.104565.
[38] Mohammadreza Nademi Rostami, Saeed Dinarvand, Ioan Pop, Dual solutions for mixed convective stagnation-point flow of an aqueous silica–alumina hybrid nanofluid, Chin. J. Phys. 56 (5) (2018) 2465–2478, https://doi.org/10.1016/j.cjph.2018.06.013.
[39] Najiyah Safwa Khashi'ie, Norihan Md Arifin, Ioan Pop, Non-Darcy mixed convection of hybrid nanofluid with thermal dispersion along a vertical plate embedded in a porous medium, Int. Commun. Heat Mass Transf. 118 (2020) 104866, https://doi.org/10.1016/j.icheatmasstransfer.2020.104866.
[40] Mohammad Ghalambaz, Natalia C. Roşca, Alin V. Roşca, Ioan Pop, Mixed convection and stability analysis of stagnation-point boundary layer flow and heat transfer of hybrid nanofluids over a vertical plate, Int. J. Numer. Methods Heat Fluid Flow. 30 (7) (2019) 3737–3754, https://doi.org/10.1108/HFF-08-2019-0661.
[41] M.R. Khan, K. Pan, A.U. Khan, S. Nadeem, Dual solutions for mixed convection flow of SiO_2- Al_2O_3/water hybrid nanofluid near the stagnation point over a curved surface, Phys. Stat. Mech. Its Appl. (2020), https://doi.org/10.1016/j.physa.2019.123959 123959.
[42] A. Jamaludin, K. Naganthran, R. Nazar, I. Pop, MHD mixed convection stagnation-point flow of Cu-Al_2O_3/water hybrid nanofluid over a permeable stretching/shrinking surface with heat source/sink, Eur. J. Mech. - BFluids. 84 (2020) 71–80, https://doi.org/10.1016/j.euromechflu.2020.05.017.
[43] N.A. Zainal, R. Nazar, K. Naganthran, I. Pop, MHD mixed convection stagnation point flow of a hybrid nanofluid past a vertical flat plate with convective boundary condition, Chin. J. Phys. 66 (2020) 630–644, https://doi.org/10.1016/j.cjph.2020.03.022.
[44] Iskandar Waini, Anuar Ishak, Ioan Pop, Mixed convection flow over an exponentially stretching/shrinking vertical surface in a hybrid nanofluid, Alex. Eng. J. 59 (3) (2020) 1881–1891, https://doi.org/10.1016/j.aej.2020.05.030.
[45] Najiyah Safwa Khashi'ie, Norihan Md Arifin, Ioan Pop, Mixed Convective Stagnation Point Flow towards a Vertical Riga Plate in Hybrid Cu-Al_2O_3/Water Nanofluid, Mathematics. 8 (6) (2020) 912, https://doi.org/10.3390/math8060912.
[46] N.S. Khashi'ie, N.M. Arifin, J.H. Merkin, R.I. Yahaya, I. Pop, Mixed convective stagnation point flow of a hybrid nanofluid toward a vertical cylinder, Int. J. Numer. Methods Heat Fluid Flow. ahead-of-print (2021). http://doi.org/10.1108/HFF-11-2020-0725.
[47] Ubaidullah Yashkun, Khairy Zaimi, Anuar Ishak, Ioan Pop, Rabeb Sidaoui, Hybrid nanofluid flow through an exponentially stretching/shrinking sheet with mixed convection and Joule heating, Int. J. Numer. Methods Heat Fluid Flow. 31 (6) (2021) 1930–1950, https://doi.org/10.1108/HFF-07-2020-0423.
[48] Y.H. Krishna, P. Bindu, N. Vijaya, G.V.R. Reddy, Radiation and chemical reaction effects on the boundary layer mhd casson fluid on a vertical plate embedded in the porous medium, Int. J. Mech. Eng. Technol. 10 (n.d.) 1–12.
[49] S. Rosseland, Astrophysik auf atomtheoretischer Grundlage, J. Springer, Berlin, 1931.
[50] Rafael Cortell Bataller, Radiation effects in the Blasius flow, Appl. Math. Comput. 198 (1) (2008) 333–338, https://doi.org/10.1016/j.amc.2007.08.037.
[51] Eugen Magyari, Asterios Pantokratoras, Note on the effect of thermal radiation in the linearized Rosseland approximation on the heat transfer characteristics of various boundary layer flows, Int. Commun. Heat Mass Transf. 38 (5) (2011) 554–556, https://doi.org/10.1016/j.icheatmasstransfer.2011.03.006.
[52] Hakan F. Oztop, Eiyad Abu-Nada, Numerical study of natural convection in partially heated rectangular enclosures filled with nanofluids, Int. J. Heat Fluid Flow. 29 (5) (2008) 1326–1336, https://doi.org/10.1016/j.ijheatfluidflow.2008.04.009.
[53] Krishnendu Bhattacharyya, G.C. Layek, Similarity solution of MHD boundary layer flow with diffusion and chemical reaction over a porous flat plate with suction/blowing, Meccanica. 47 (4) (2012) 1043–1048, https://doi.org/10.1007/s11012-011-9461-x.
[54] Swati Mukhopadhyay, Iswar Chandra Mandal, Magnetohydrodynamic (MHD) mixed convection slip flow and heat transfer over a vertical porous plate, Eng. Sci. Technol. Int. J. 18 (1) (2015) 98–105, https://doi.org/10.1016/j.jestch.2014.10.001.
[55] J.H. Merkin, On dual solutions occurring in mixed convection in a porous medium, J. Eng. Math. 20 (2) (1986) 171–179, https://doi.org/10.1007/BF00042775.
[56] P.D. Weidman, D.G. Kubitschek, A.M.J. Davis, The effect of transpiration on self-similar boundary layer flow over moving surfaces, Int. J. Eng. Sci. 44 (11-12) (2006) 730–737, https://doi.org/10.1016/j.ijengsci.2006.04.005.
[57] S.D. Harris, D.B. Ingham, I. Pop, Mixed Convection Boundary-Layer Flow Near the Stagnation Point on a Vertical Surface in a Porous Medium: Brinkman Model with Slip, Transp. Porous Media. 77 (2) (2009) 267–285, https://doi.org/10.1007/s11242-008-9309-6.
[58] F.B. Tadesse, O.D. Makinde, L.G. Enyadene, Hydromagnetic stagnation point flow of a magnetite ferrofluid past a convectively heated permeable stretching/shrinking sheet in a Darcy-Forchheimer porous medium, Sādhanā. 46 (2021) 115, https://doi.org/10.1007/s12046-021-01643-y.
[59] Khodani Sherrif Tshivhi, Oluwole Daniel Makinde, Magneto-nanofluid coolants past heated shrinking/stretching surfaces: Dual solutions and stability analysis, Results Eng. 10 (2021) 100229, https://doi.org/10.1016/j.rineng.2021.100229.
[60] L. Howarth, L. Bairstow, On the solution of the laminar boundary layer equations, Proc. R. Soc. Math. Phys. Eng. Sci. 164 (1938) 547–579, https://doi.org/10.1098/rspa.1938.0037.